Molecular Psychiatry (2018) 23, 1868–1877
www.nature.com/mp

OPEN

ORIGINAL ARTICLE

Corticostriatal circuit defects in *Hoxb8* mutant mice

N Nagarajan[1], BW Jones[2], PJ West[3], RE Marc[2] and MR Capecchi[1]

Hoxb8 mutant mice exhibit compulsive grooming and hair removal dysfunction similar to humans with the obsessive-compulsive disorder (OCD)-spectrum disorder, trichotillomania. As, in the mouse brain, the only detectable cells that label with *Hoxb8* cell lineage appear to be microglia, we suggested that defective microglia cause the neuropsychiatric disorder. Does the *Hoxb8* mutation in microglia lead to neural circuit dysfunctions? We demonstrate that *Hoxb8* mutants contain corticostriatal circuit defects. Golgi staining, ultra-structural and electrophysiological studies of mutants reveal excess dendritic spines, pre- and postsynaptic structural defects, long-term potentiation and miniature postsynaptic current defects. *Hoxb8* mutants also exhibit hyperanxiety and social behavioral deficits similar to mice with neuronal mutations in Sapap3, Slitrk5 and Shank3, reported models of OCD and autism spectrum disorders (ASDs). Long-term treatment of *Hoxb8* mutants with fluoxetine, a serotonin reuptake inhibitor, reduces excessive grooming, hyperanxiety and social behavioral impairments. These studies provide linkage between the neuronal defects induced by defective *Hoxb8*-microglia and neuronal dysfunctions directly generated by mutations in synaptic components that result in mice, which display similar pathological grooming, hyperanxiety and social impairment deficits. Our results shed light on *Hoxb8* microglia-driven circuit-specific defects and therapeutic approaches that will become essential to developing novel therapies for neuropsychiatric diseases such as OCD and ASDs with *Hoxb8*-microglia being the central target.

Molecular Psychiatry advance online publication, 26 September 2017; doi:10.1038/mp.2017.180

INTRODUCTION

Grooming is an evolutionarily well-conserved innate behavior of rodents and other mammalian species that is essential for survival. The grooming circuit induces hierarchically ordered set of actions, which in *Hoxb8* mutants are characterized by compulsive excessive grooming, hair removal and lesions at the sites of overgrooming.[1–5] *Hoxb8* mutant analysis suggested that defective microglia underlie the behavioral deficits.[4] How *Hoxb8* gene disruption alters neural circuit, induces behavioral dysfunctions and cause neuronal pathology has neither been addressed nor has such ensuing neural damage been previously defined. Functional imaging in humans[6–8] and genetic mutational studies in *SAPAP3*, *Slitrk5* and *Shank3* mutant[9–11] mice has pointed to corticostriato-thalamo-cortical circuit defects as a basis for obsessive-compulsive disorder (OCD) pathogenesis.[12–17]

To address the role of *Hoxb8* gene function in neuronal pathology we examined neuronal integrity of *Hoxb8* mutants and evaluated corticostriatal structural and functional synaptic impairments. We further demonstrate that *Hoxb8* mutants exhibit anxiety and social interaction behavioral dysfunction in addition to pathological grooming. These behaviors in mutants are rescued by long-term fluoxetine treatment similar to humans.[18] This work ties together *Hoxb8* gene-induced neural pathology with the neural *SAPAP3*, *SlitrK5* and *Shank3* mutant[9–11] mice models of OCD and autism spectrum disorder (ASD). We infer that the *Hoxb8* gene in the *Hoxb8* cell lineage normally modulate the corticostriatal circuit and controls grooming behavior. The absence of *Hoxb8* function in microglia leads to aberrant modulation and physical impairment of these neural circuits leading to OCD-like compulsive behavior in mice.

MATERIALS AND METHODS

All experiments were approved by the The Institutional Animal Care and Use Committee, University of Utah.

Electron microscopy

Tissues were fixed (24 h) in 1% formaldehyde, 2.5% glutaraldehyde, 3% sucrose and 1 mM $MgSO_4$ in 0.1 M cacodylate buffer, osmicated (60 min) in 0.5% OsO_4 in 0.1 M cacodylate buffer, processed in maleate buffer for en bloc staining with uranyl acetate and processed for resin embedding.[19] Sixty to 90 nm sections were mounted onto Formvar Films (Ted Pella, Redding, CA, USA) and imaged (GATAN Ultrascan 4000, Pleasanton, CA, USA) at 80 KeV (JEOL, Peabody, MA, USA, JEM-1400-EM, ×5000 magnification and nanometer resolution) from $1 \times 1 \times 1$ mm^3 tissue volume. IR tools mosaicked transmission electron microscopy data and corrected aberrations and electron-optical distortions after mosaic construction on individual tiles. All statistics used for electron microscopy analysis per sample per genotype and grouped analysis is summarized in Supplementary Table 2. Sample size for data analysis was determined by power analysis and literature.[9,11] Spine and synapse quantification was performed by an experimenter blinded to genotype and the brain region.

Slice electrophysiology

Slices from isolated brains were placed in ice-cold (4 °C) oxygenated sucrose-based artificial cerebral spinal fluid (ACSF) (95% O_2/5% CO_2) containing (in mM): sucrose (180.0), KCl (3.0), Na_2PO_4 (1.4), $MgSO_4$ (3.0), $NaHCO_3$ (26.0), glucose (10.0) and CaCl2 (0.5). ACSF contained (in mM): NaCl (126.0), KCl (3.0), Na_2PO_4 (1.4), $MgSO_4$ (1.0), $NaHCO_3$ (26.0), glucose (10.0) and $CaCl_2$ (2.5) (pH 7.3–7.4, 290–300 mOsm).

Corticostriatal long-term potentiation

Field excitatory postsynaptic potentials were recorded (30–31 °C) from slices perfused with oxygenated ACSF (2.5 ml min^{-1}). Concentric bipolar

[1]Department of Human Genetics, University of Utah School of Medicine, Salt Lake City, UT, USA; [2]John A. Moran Eye Center, Department of Ophthalmology and Visual Sciences, University of Utah School of Medicine, Salt Lake City, UT, USA and [3]Department of Pharmacology and Toxicology, University of Utah, Salt Lake City, UT, USA. Correspondence: Dr N Nagarajan or Professor MR Capecchi, Department of Human Genetics, University of Utah School of Medicine, 15N, 2030 East, Room 5440, Salt Lake City, UT 84112, USA. E-mail: naveen@genetics.utah.edu or capecchi@genetics.utah.edu
Received 22 February 2017; revised 6 June 2017; accepted 30 June 2017

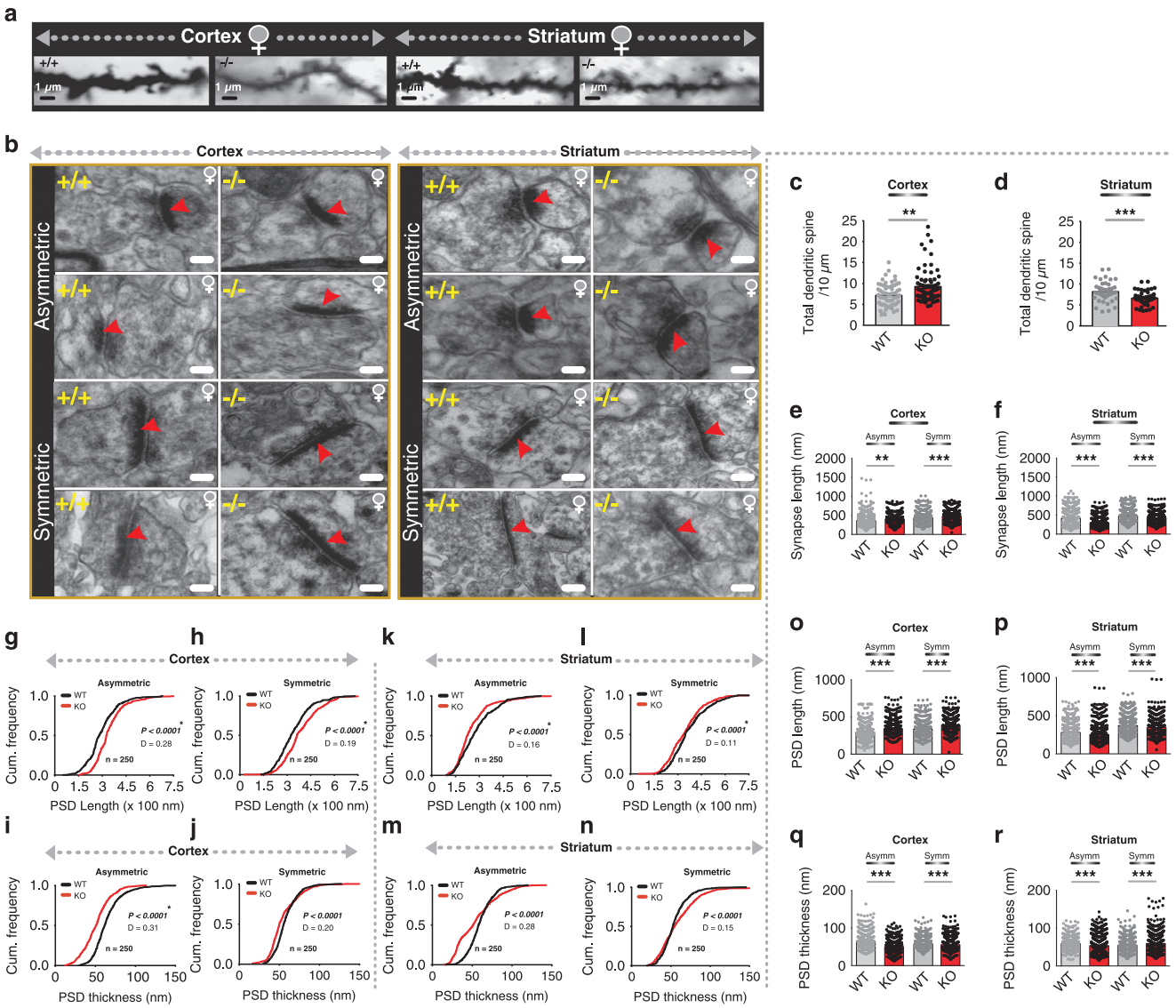

Figure 1. Altered cortical and striatal synapses in *Hoxb8* mutants. (**a**) Representative dendritic spines from 6 months old wild-type (WT) and *Hoxb8* female mutant mice from frontal cortical and dorsal striatal regions. Scale bar: 1 μm. (**b**) Representative electron microscopic images of cortical-asymmetric, cortical-symmetric, striatal-asymmetric and striatal-symmetric synapses from 6 months old WT and *Hoxb8* mutant brains, and visualized using Viking software.[19,53] Scale bar: 100 nm. (**c** and **d**) Significantly increased cortical ($P = 0.0034$, $F = 9.118$, 28 WT and 29 mutant neurons, 2–3 healthy dendrites per neuron) (**c**) but decreased (**d**) striatal spine density ($P = 0.001$, $F = 10.488$, 13 WT and 18 mutant neurons, 2–3 healthy dendrites per neuron) in female *Hoxb8* mutants (3 litters per group, 8 months old mice) using golgi staining (Fd Neurotechnologies, Inc.). (**e** and **f**) Bar plot displaying significantly increased synapse length at cortical asymmetric ($P = 0.00012$, $F = 14.8310$) and symmetric ($P < 0.0001$, $F = 19.8205$) (**e**) but a significantly decreased striatal asymmetric ($P < 0.0001$, $F = 138.0321$) and symmetric synapses ($P < 0.0001$, $F = 37.9242$) (**f**). (**g**–**j**) Cumulative probability plot demonstrating a significant rightward shift in the PSD length in *Hoxb8* mutants compared to WT mice (**g**, $P < 0.0001$, $D = 0.2815$; **h**, $P < 0.0001$, $D = 0.1992$) but a significant leftward shift in PSD thickness for cortical asymmetric and cortical symmetric synapses (**i**, $P < 0.0001$, $D = 0.3187$; **j**, $P < 0.0001$, $D = 0.2045$). (**k**–**n**) A contrasting significant decrease (leftward shift) within striatal-asymmetric (**k**, $P < 0.0001$, $D = 0.1595$) and symmetric (**l**, $P < 0.0001$, $D = 0.1156$) synapses for PSD length and PSD thickness (**m**, $P < 0.0001$, $D = 0.28$; **n**, $P < 0.0001$, $D = 0.15$). (**o** and **p**) Bar graph representation of significantly increased PSD length at cortical-asymmetric ($P < 0.0001$, $F = 93.2869$) and cortical-symmetric ($P < 0.0001$, $F = 53.6979$) (**o**) synapses of *Hoxb8* mutants but a contrasting decrease within striatal-asymmetric (**p**) ($P < 0.0001$, $F = 22.1849$) and striatal-symmetric synapses (**p**) ($P < 0.0001$, $F = 18.1742$). (**q** and **r**) Bar graph representation of significantly decreased PSD thickness at cortical-asymmetric ($P < 0.0001$, $F = 192.3888$) and cortical-symmetric ($P = 0.014$, $F = 5.9328$) (**q**) synapses of *Hoxb8* mutants but a contrasting increase within striatal-asymmetric ($P < 0.0001$, $F = 30.8782$) and striatal-symmetric ($P < 0.0001$, $F = 17.4861$) (**r**) synapses. Red arrow represents postsynaptic density in individual synapse. All analysis was conducted on WT and *Hoxb8* mutant female mice brains. One-way analysis of variance and Tukey's *post-hoc* test (**c**–**f** and **o**–**r**). Kolmogorov–Smirnov test (**g**–**n**).

stimulating electrodes were placed in dorsomedial striatum at its interface with corpus callosum.[20–22] Recording microelectrodes were placed near (250 μm) stimulating electrodes in dorsomedial striatum. Field excitatory postsynaptic potentials were evoked with 100 μs stimuli (1–40 V, stimulation strength 50% of minimal and maximal field excitatory postsynaptic potential amplitudes).

Whole-cell recordings

Acute brain slices (300 μm thickness) were cut and recovered (45–60 min) in a submerged chamber (31 °C) with ACSF (in mM) 125 NaCl, 2.5 KCl, 2.0 $CaCl_2$, 1 $MgCl_2$, 1.25 NaH_2PO_4, 25 $NaHCO_3$ and 15 D-glucose (pH 7.4, 300–310 mOsm), and perfused with oxygenated (95% O_2/5% CO_2) ACSF at 2 ml min^{-1} at 31 °C. Internal solution was (in mM) 107 $CsMeSO_3$, 10 CsCl,

3.7 NaCl, 5 TEA-Cl, 20 HEPES, 0.2 EGTA, 5 lidocaine, 4 ATP-magnesium and 0.3 GTP-sodium salt (pH 7.3, 298–301 mOsm). Data were sampled at 10 kHz with low- and high-pass filter set to 1 kHz and 3 Hz. Sample size for data analysis was determined by power analyiss and literature. Sample size for all electrophysiological experiments was determined based on the literature.[9–11,20–23]

Grooming behavior. Grooming assay used vibration-sensitive platforms and Laboras software (Hoofddorp, The Netherlands) for data analysis. Parameters extracted from grooming assay is shown in Supplementary Table 3 and statistical summary is provided in Supplementary Table 5.

Elevated plus maze, open-field and light-dark test

Anxiety was tested in plus maze ($5 \times 35 \times 15 \times 40$ cm), open-field ($40 \times 40 \times 35$ cm) and light-dark arena ($40 \times 40 \times 35$ cm). Mouse movement was tracked using ANY-Maze software (Stoelting, Wood Dale, IL, USA). Parameters extracted from anxiety assay are shown in Supplementary Table 4 and statistical summary is provided in Supplementary Table 5.

Three-chambered social assay. Thirty-minute social assay was performed in three-chambered compartment. Test mouse was placed in center while intruder mouse in right with left chamber being empty. After placing test mouse at the center for 10 min habituation, left and right doors were opened for test mouse to interact with empty or intruder chamber. Test mice movements were tracked using Laboras. Statistical summary is provided in Supplementary Table 5.

Fluoxetine treatment

Mice that underwent fluoxetine or saline treatment were acclimated in home cages for >7 days. Wild-type (WT) and mutants were intraperitoneally injected (5 mg kg^{-1}) with fluoxetine once a day for 1 day, 1, 5 and 13 weeks. Sample size for all behavioral and drug treatment conditions were determined by literature[9–11] and power analysis. Statistical summary is provided in Supplementary Table 5.

All behavioral experiments were conducted blindly with the experimenter blind to genotype and drug treatment conditions.

RESULTS

Hoxb8 mutants show altered pre- and postsynaptic structures

We first determined whether *Hoxb8* mutants show altered corticostriatal synapse morphology similar to those shown to be defective in SAPAP3 and Slitrk5 mutant mice, well-studied mouse models of OCD. We measured dendritic spine density in frontal cortical and striatal neurons using Golgi–Cox staining. Mutants exhibit significantly higher spine density in the frontal cortex but lower density in the striatum (Figures 1a, c and d) implying distinct effects of *Hoxb8* mutation on spine maintenance within cortex and striatum. Spines averaged per mouse reproduced the average value (Supplementary Table 1d–e). To identify the dendritic spine density changes in OCD-specific striatal brain regions, as opposed to global spine density changes in the entire striatum, we quantified spine density from dorso and ventro-medial striatum of WT and *Hoxb8* mutants. Spine density in *Hoxb8* mutants increased significantly in both dorso- and ventro-medial striatal regions (Supplementary Figures 1c, e, d and f) without affecting spine density from the visual cortex (Supplementary Figures 1b and g), a control brain region that is independent of OCD circuit. These data suggests that distinct striatal sub-regions show diverse dendritic spine phenotype.

To identify whether the *Hoxb8* mutation affects synaptic structures, we examined asymmetric (excitatory) and symmetric (inhibitory) cortical and striatal synapses using electron microscopy. Representative synapses are displayed and modeled (Figure 1b and Supplementary Figure 3a). At asymmetric and symmetric cortical synapses, synaptic length increased significantly compared with WT (Figure 1e and Supplementary Figures 2m and n). Contrastingly, synaptic length decreased significantly at striatal asymmetric and symmetric synapses (Figure 1f and Supplementary Figures 2o and p), suggesting defective but contrasting cortical and striatal structural synapse in mutants. To determine postsynaptic alteration, we quantified postsynaptic density (PSD) length and thickness. PSD length in mutants shifted rightward (Figures 1g and h) in cumulative distribution and was significantly longer at asymmetric and symmetric cortical synapses (Figure 1o). Contrastingly, PSD thickness of asymmetric and symmetric cortical synapses of mutants shifted leftward in cumulative distribution (Figures 1i and j) and were significantly smaller than WT (Figure 1q). Synaptic expansion in mutants concurrently increased pre-synaptic diameter at asymmetric and symmetric synapses, but expanded postsynaptic diameter only at asymmetric synapses (Supplementary Figures 3b–e, j and l, and Supplementary Table 1). To identify whether synaptic structural changes affect active zone, we quantified active zone length and thickness at cortical synapses. Mutants exhibit longer active zones at asymmetric and symmetric synapses (Supplementary Figures 2a, b and i, and Supplementary Table 1). Changes in the active zone thickness were insignificant at either of the synapses (Supplementary Figure 2k), although cumulative distribution showed statistical significance for symmetric synapses (Supplementary Figures 2d and c, and Supplementary Table 1). Together the data imply that the *Hoxb8* mutation affects the cortical pre- and postsynapses and results in synaptic expansion at asymmetric and symmetric synapses. As we detected synaptic expansion within frontal cortical synapses, we asked whether such structural alteration result in more or stronger synapses? We analyzed total excitatory and inhibitory synapses within frontal cortex and observed that mutants exhibit significantly increased mono- and total asymmetric but not symmetric synapses (Supplementary Figures 2q–t) implying increased synaptic density in mutants in consistence with synaptic structural modification.

In contrast to cortex, *Hoxb8* mutants showed a significant reduction of PSD length (Figure 1p) and shifted cumulative distribution leftward at asymmetric (Figure 1k) and symmetric (Figure 1l) striatal synapses. PSD thickness of asymmetric and symmetric striatal synapses in mutants was significantly greater than WT (Figure 1r) and shifted cumulative distribution rightward (Figures 1m and n). Synaptic contraction concurrently reduced pre and postsynaptic diameter with leftward shifting of cumulative distribution (Supplementary Figures 3f–i, k and m, and Supplementary Table 1). Similar to pre- and postsynaptic contraction, mutants exhibit smaller active zones at asymmetric and symmetric synapses (Supplementary Figures 2e, f and j, and Supplementary Table 1). Contrast to cortex, active zone thickness shrunk at asymmetric but expanded significantly at symmetric striatal synapses (Supplementary Figures 2g, h and l, and Supplementary Table 1), indicating that *Hoxb8* mutation affects striatal and cortical synapses differentially (Supplementary Tables 1c and 2). Synaptic analysis revealed a significant increase in mono and total synapses at asymmetric excitatory but reduced mono and total synapses at symmetric synapses (Supplementary Figures 2u–x) in mutants consistent with the synaptic structural modification at cortical and striatal synapses in *Hoxb8* mutants, leading to an increased excitation at the corticostriatal circuit as has been reported for SAPAP3, Slitrk5 and Shank3 mutant mice.[9–11]

Altered CNQX-insensitive long-term potentiation and miniature excitatory currents in *Hoxb8* mutants

We investigated whether altered pre- and postsynaptic structure observed in frontal cortex and striatum affected corticostriatal neurotransmission in *Hoxb8* mutants. The input–output curves, slope normalized to peak response, field potential amplitudes and paired-pulse ratio at striatal synapses revealed insignificant difference between mutant and WT slices (Supplementary Figures 4a–c and Figure 2a) in response to layer 5/6 cortical fiber stimulation implying that the electrophysiological properties and short-term plasticity is intact in mutants.

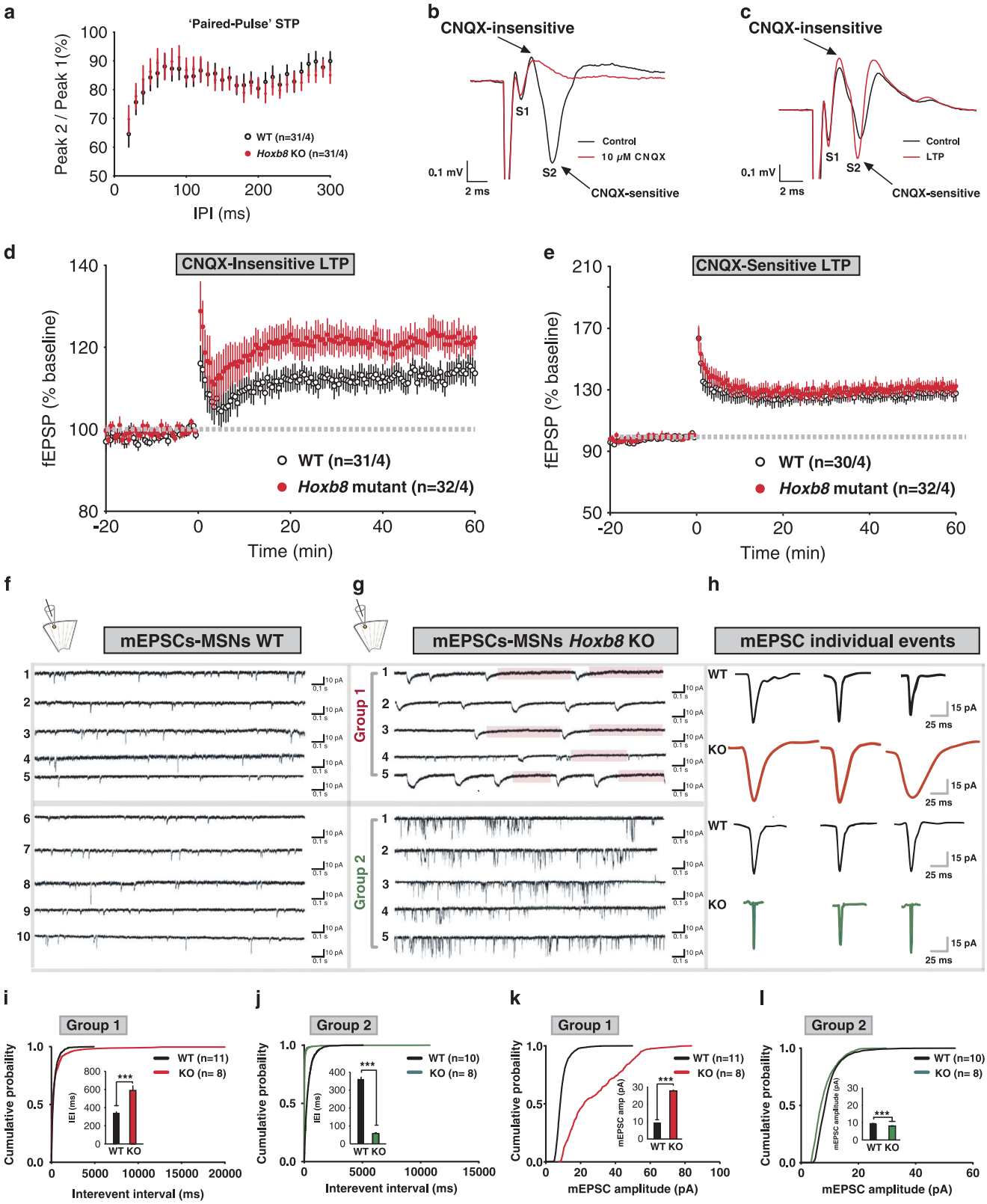

To probe presynaptic plasticity, population spike responses were measured in dorsal striatum. Single pulse layer 5/6 cortical stimulation evoked a population spike that was dependent on synaptic glutamate release and postsynaptic AMPA (α-amino-3-hydroxy-5-methyl-4-isoxazolepropionic acid receptor)/kainate receptors.[20] Population spike consisted of non-synaptic (S1, source current) presynaptic component and synaptically mediated postsynaptic component (S2, sink current)[20–22,24] (Figures 2b and c). Because of non-laminar striatal organization, sink and source currents (a) overlap in space, (b) arise from action

Figure 2. Altered CNQX independent form of long-term potentiation (LTP) and miniature EPSCs in *Hoxb8* mutants at corticostriatal synapses. (**a)** Paired-pulse ratio is unchanged in mutants ($P = 0.3453$, F (28, 1680) = 1.086 for interaction; $P < 0.0001$, F (28,1680) = 10.09 for interpulse interval, $P = 0.9560$, F(1, 60) = 0.003074 for genotype; $P < 0.0001$, F(60,1680) = 76.89 for subjects matching). Paired-pulse ratio of the field excitatory postsynaptic potential (fEPSP) amplitudes was assessed using inter-pulse intervals between 20–300 ms in 10 ms intervals. Single stimuli were given to slices every 30 s for a 30 min to collect baseline. Representative traces and measurements are the average from five consecutive traces. (**b)** Representative trace of field potentials in ± CNQX condition (black and red trace). S1, non-synaptic and S2, synaptically mediated component. Overlaid traces show the sensitivity of S1 and S2 component to CNQX. (**c)** Overlaid trace of field potential recording under control (black) and LTP (red) condition showing S1 and S2 components. Scale bar, 0.1 mV (*Y* axis) and 2 ms (*X* axis). (**d)** Increased CNQX-insensitive LTP for WT (black) and mutants (red) ($P = 0.1665$, F (60, 3300) = 1.177 for interaction; $P = 0.0014$, F(60, 3300) = 1.642 for interpulse interval, $P = 0.0378$, F(1, 55) = 4.531 for genotype; $P < 0.0001$, F (55, 3300) = 524.5 for matched subjects). LTP was induced by high frequency stimulation (1 s/100 Hz). Low-frequency stimulation was resumed for 60 min to quantify LTP relative to baseline. (**e)** Normal CNQX-sensitive LTP for WT (black) and mutants (red) ($P = 0.9477$, F(60, 3060) = 0.7213 for interaction; $P = 0.0316$, F(60, 3060) = 1.371 for time; $P = 0.558$, F(1, 51) = 0.3471 for genotype and $P < 0.0001$, F(51, 3060) = 476.7 for matched subjects, two-way analysis of variance (ANOVA) repeated measures). Significance was determined at $P < 0.05$. Data were excluded if the slope of fEPSPs during the 30 min baseline changed by > 20%. (**f** and **g**) AMPA receptor mediated miniature evoked postsynaptic current (mEPSC) recording traces at -70 mV from dorsomedial striatal MSNs from parasiggital corticostriatal acute brain slices for WT (left) and *Hoxb8* mutants (n = 3 mice per genotype, 3 week old) isolated in the presence of TTX (1 μM), DL-2-amino-5-phosphonovaleric acid (50 μM), D-Serine (10 μM), Picrotoxin (100 μM) and Gabazine (5 μM) to block action potential, NMDA, GABA and GABAA receptors, respectively, in whole-cell voltage clamp recording configuration. Based on kinetics, the electrophysiological property of mEPSC events such as decay time and frequency, the responses from *Hoxb8* mutants were classified into group 1 and 2. Orange and green bars on the traces represent time periods where no mEPSC activity was detected. Cartoon on the top shows the location of pipette positioning and recording within the striatum. (**h**) mEPSC individual representative events for WT and *Hoxb8* mutants from group 1 and group 2 type of MSN neuronal responses. The amplitude varied among individual events. Small, medium and large amplitude events were recorded and analyzed. (**i**–**l**) Cumulative probability plot of WT and *Hoxb8* mutants showing rightward shift in the curve for *Hoxb8* mutants for inter-event interval and mEPSC amplitudes for group 1 (**i**, $P = 0.002$, $D = 0.08375$; $P = 0.00029$, F = 13.18906 for inset; **k**, $P < 0.0001$, $D = 0.6917$; $P < 0.0001$, F = 2654.712 for inset) and group 2 neurons (**j**, $P < 0.0001$, $D = 0.7023$; $P < 0.0001$, F = 949.241; **l**, $P < 0.0001$, $D = 0.2040$; $P < 0.0001$, F = 111.279 for inset). Inset represents bar graph from the same data set. '*n*' represents the number of neurons patched per experimental group obtained from three WT and three *Hoxb8* mutants. Atleast 100 events were sampled per neuron. Series and input resistance were monitored continuously and neuronal recordings were discarded if these parameter changed by > 20%. All experiments were conducted blindly in which the experimenter was unaware of the electrophysiological outcome of different cell types within dorsal striatum. mEPSCs were analyzed using Minianalysis Synaptosoft software. One-way ANOVA and Tukey's *post-hoc* test for bar graphs, Kolmogorov–Smirnov test (**i**–**l**). Six months old WT and *Hoxb8* mutant brain slices were used for the slice electrophysiological experiments.

potentials with shorter latency and (c) are CNQX-insensitive and interchangeable measures of presynaptic depolarization.

In control experiments, CNQX, (AMPA/kainate receptor antagonist) blocked the S2 but not S1 component (Figure 2b), indicating that the action potential dependent component is CNQX-sensitive (S2), whereas the independent component is CNQX-insensitive (S1). To investigate whether mutants show changes in S2 versus S1, tetanic stimulation was applied to dorsomedial striatum and long-term potentiation was measured. Strikingly, the S1 increased significantly in mutants compared with WT (Figure 2d) without affecting the S2 (Figure 2e), suggesting that the loss of the *Hoxb8* gene affects CNQX-independent (cortical driven) but not CNQX-dependent (intra-striatal) long-term potentiation. S1 versus S2 field potential amplitudes did not differ significantly (Supplementary Figure 4d), implying that the postsynaptic striatal output is smaller despite presynaptic changes consistent with the reduced spine density, synapse and PSD length of mutants (Figures 1d, f and p) at striatal synapses analyzed.

As cortical and striatal spine density and PSD morphology was altered, we questioned whether electrophysiological signature of such synaptic change exist in dorsomedial striatum. We recorded AMPA-receptor-mediated excitatory miniature evoked postsynaptic currents (mEPSCs) from dorsal medium spiny neurons (MSNs). Two distinct mEPSC types were detected in MSNs of mutants that were distinguishable by response kinetics and decay time, and categorized into slow (Group 1) and fast (Group 2) miniature events (Figures 2g and h, and Supplementary Figure 4f). Representative events are displayed in Figure 2h. Group 1 MSNs of mutants exhibit significantly longer inter-event interval with higher amplitudes (Figures 2g, i and k), whereas group 2 MSNs showed significantly reduced inter-event interval and mEPSC amplitudes relative to WT mice (Figures 2g, j and l), implying that the probability of the presynaptic neurotransmitter release and postsynaptic AMPA receptors might be affected in opposite way. These effects were prominent when rise and decay times (Supplementary Figures 4g–j), mEPSC charge, event half-width (Supplementary Figures 4k–n) and frequency (Supplementary Figures 5a and b) were analyzed. The relationship between (a) mEPSC amplitude and 10–90% rise time (Supplementary Figures 5c and d), (b) amplitude and average rise rate (Supplementary Figures 5e and f) and (c) event half width and 10–90% rise time (Supplementary Figures 5g and h) were distinguishable between WT and mutants. These data imply that mEPSC events of MSNs are affected in mutants at single neuronal level.

Hoxb8 mutants show impaired grooming, anxiety and social behaviors

To determine the role of *Hoxb8* mutation in grooming, we used 24 h automatic Laboras platform containing sensitive vibration detectors to detect grooming and non-grooming behaviors.[23] Reproducibly,[3,4] Laboras detected significantly higher self-grooming behavior in mutants compared to WT mice (Figure 3a and Supplementary Tables 3).

Two features common to OCD and ASD are hyperanxiety and social behavioral deficits.[9–11,15] We investigated whether such behaviors in mutants are altered. In plus maze test, mutants spent significantly more time in closed arm compared with WT mice (Figures 3b and c) without altering distance in closed arm (Supplementary Figure 6a), implying that mutants are more anxious in plus maze. Mutants spent significantly decreased time in open arm under different light intensities (1.7-fold at 75 lx, 2.7-fold at 100 lx; Supplementary Figure 6b), traveled for shorter distances (1.5-fold, 75 lx; 3.2-fold, 100 lx; Supplementary Figure 6c) and had longer latencies (3.7-fold, 75 lx; 4.9-fold, 100 lx; Supplementary Figure 6d) than controls.

In open-field test, an additional indicator of anxiety level, mutants exhibit significantly reduced- time at the center (Figures 3d and e), line crossings, entries and circling numbers (Supplementary Figures 6f and e), implying higher anxiety levels relative to controls. Both male and female mutants showed higher anxiety levels (Supplementary Table 4). In light–dark test,

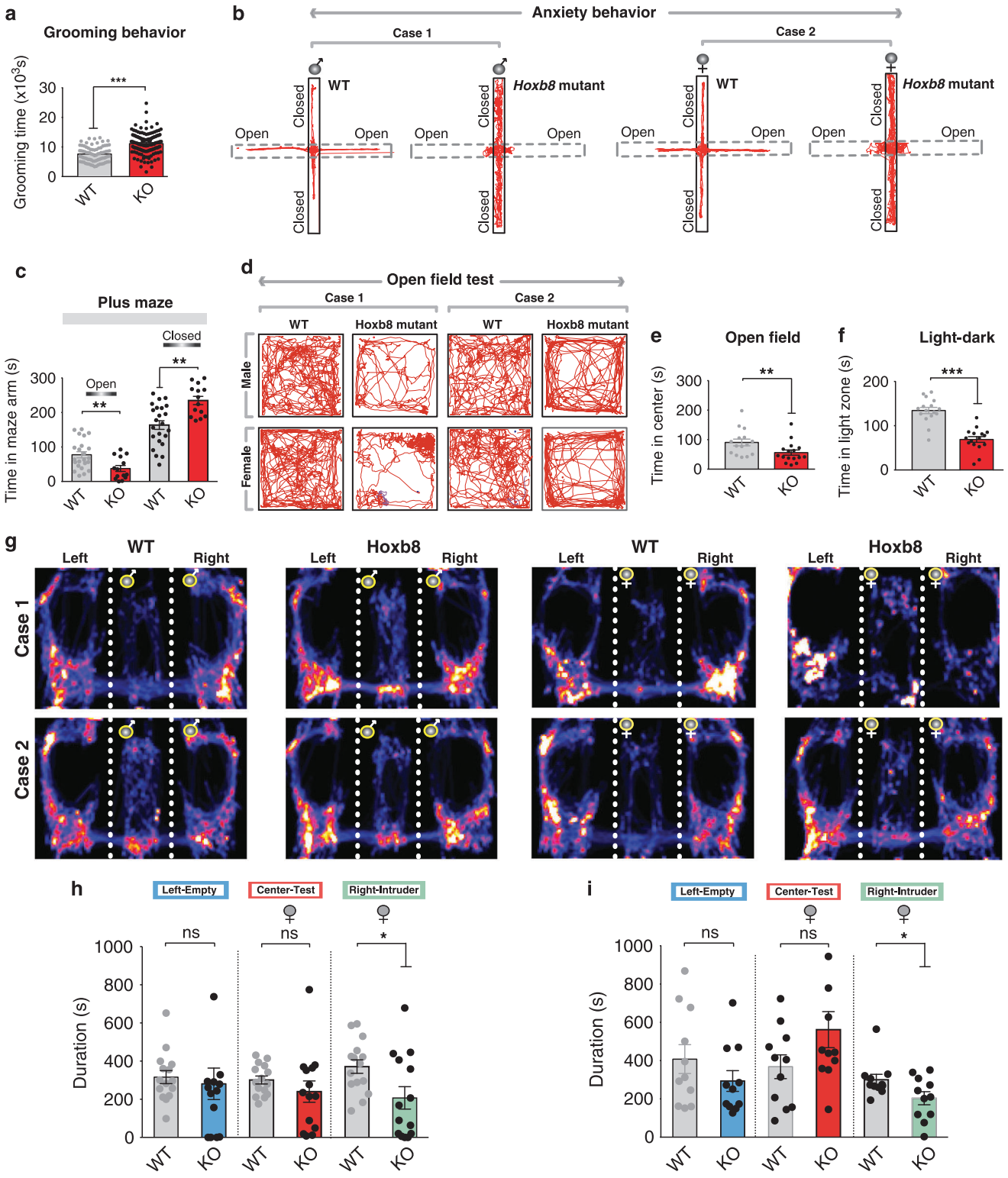

mutants spent reduced time in light (Figure 3f) and more time in dark chamber (Supplementary Figure 6h) compared with WT mice without affecting the total light zone entries (Supplementary Fig. 6i). All these anxiety tests suggested that *Hoxb8* mutants exhibit hyperanxiety levels relative to controls.

We tested social behaviors in *Hoxb8* mutants using a three-chambered social assay in which the test subject (WT or mutant, male or female) is placed at the center, with an empty left chamber and an intruder mouse in the right chamber. Mutants spent significantly reduced time socially interacting with the intruder (Figure 3h). Heat maps derived from male and female mutants (Figure 3g) during social assay show evidence that female mutants exhibit significantly higher social impairment compared with males. To determine whether mutants interact normally with

Figure 3. Altered grooming, anxiety and social behaviors in *Hoxb8* mutants. (**a**) Mutants show increased grooming ($P < 0.0001$, $F = 59.115628$) in 24 h grooming assay as compared with WT mice (4–12 months old). (**b**) Representative track plots of male WT, male mutants, female WT and female mutants in 5 min elevated plus maze test under ambient light conditions. It is noteworthy that the movement of mutants pertained to closed as compared with open chamber. (**c**) *Hoxb8* mutants (6–8 months old) spend reduced time in open ($P = 0.00474$, $F = 9.10139$) and increased time in closed arm ($P = 0.0005$, $F = 14.7216$) (left panel). (**d**) Representative track plots of male WT and male mutant (upper panel), female WT and female mutant (lower panel) in the open field test. (**e** and **f**) Mutants (6–8 months old) spend significantly reduced ($P = 0.02369$, $F = 5.70155$) time- at the center of the open field in a 30 min open field test and within the light zone ($P = 0.00027$, $F = 15.4018$) (right panel) in 5 min light–dark test (illumination 600 Lx). (**g**) Representative heat maps of individual male and female WT and *Hoxb8* mutants (Case 1–2) during three-chambered social interaction assay with an empty left chamber and an intruder in the right chamber (same sex as the test mouse). (**h**) Female mutants (6–8 months old) spent significantly reduced time with the intruder mouse in the right chamber ($P = 0.1148$, $F = 15.40186$ for left chamber non-contact duration; $P = 0.3004$, $F = 2.6407275$ for the total duration in the center; $P = 0.0222$, $F = 5.8829406$ for total contact duration with the intruder) in social interaction assay. Data represents mean ± s.e.m., uses one-way analysis of variance (ANOVA) and Tukey's honest significant difference (HSD) *post-hoc* test for comparison. ns, not significant $P > 0.05$, $^*P < 0.05$). (**i**) Bar graph representation of the comparison of social interaction pattern of female *Hoxb8* mutants and WT mice (6–8 months old) with an empty chamber (left) and a cage mate (right) ($P = 0.0861$, $F = 3.27635$ for the non-contact duration with the left chamber; $P = 0.427$, $F = 0.65771$ for total duration in the center; $P = 0.0095$, $F = 8.325$ for total contact duration with intruder). The cage-mate was of same age and sex as of experimental mice. All bar graph data represents mean ± s.e.m. Data comparison, one-way ANOVA and Tukey's HSD *post-hoc* test was used for group comparison. ns, $P > 0.05$ not significant, $^*P < 0.05$, $^{**}P < 0.001$. Four to 12 months old mice were used for grooming behavior, 6–8 months old mice for elevated plus maze, open-field and social behavioral tests. All test mice were conditioned for 5–15 min in specific experimental rooms prior to the experiments. All behavioral experiments were conducted during day light period of the light/dark cycle. All experiments were conducted blindly without the knowledge of experimenter to genotypes.

cage-mates, test mice were challenged to interact with a cage-mate in social assay. Mutants showed a significant social deficit even with a cage mate, a defect that was confined to the female mutants (Figure 3i and Supplementary Figure 6j), indicating that female mutants show higher detectable social impairment than males.

Fluoxetine treatment of *Hoxb8* mutants alleviates grooming, anxiety and social impairment behaviors

We evaluated whether fluoxetine ameliorates behavioral abnormalities in *Hoxb8* mutants. One week, but not 1-day treatment reduced grooming time of mutants without significantly affecting the WT mice (Supplementary Figure 7a). No sedative effect was detected as measured by locomotion and immobility between saline or fluoxetine-treated groups, implying the appropriateness of drug dosage (Figures 4b and c). To determine long-term effects of fluoxetine on anxiety, mutants and WT mice were chronically treated for five weeks. In plus maze test, treated mutants spent a 3.4-fold increased time in open-arm compared with saline-treated mutants (Figure 4d). Treated mutants that spent more time at the center of the open field compared with saline treated mutants did not reach WT levels (Figure 4e), implying a partial rescue. When exposed to a novel intruder, treated mutants compared with WT mice spent a reduced time in empty chamber and similar time at the center or with the intruder mouse (Figures 4g and h), implying that the treatment resulted in improved social behaviors. To investigate whether the alleviated behaviors are sustained during chronic fluoxetine treatment, mutants and WT mice were treated with fluoxetine upto thirteen weeks. Anxiety and exploratory locomotion were tested using light–dark and open-field tests. The distance at the center or periphery of open field (Supplementary Figures 7b and c) and the time in light zone (Supplementary Figure 7d) reached WT-like levels implying extensive rescue. Amount of time spent by mutants in light zone during light–dark exploration increased to WT levels (Figure 4f). These data demonstrate that fluoxetine treatment alleviates pathological grooming, anxiety and aberrant social behaviors in *Hoxb8* mutants.

DISCUSSION

Targeted disruption of *Hoxb8* gene causes brain-specific[3,4] compulsive hair removal behavior closely resembling the OCD spectrum disorder Trichotillomania in humans.[24] We now show that *Hoxb8* loss of function results in synaptic and physiological defects within corticostriatal circuit. This corticostriatal defect in mutants resulted in frontal cortical synaptic expansion and striatal synaptic contraction. The increased cortical synapse and spine density within frontal cortex in conjunction with increased dendritic spines in dorso- and ventro-medial sub-regions of striatum implicate a potential increase in excitatory corticostriatal synapse.

These synaptic modifications were also detectable electrophysiologically. At circuit level we detected impaired CNQX-independent striatal synaptic long-term potentiation. This plasticity may emerge from changes in presynaptic medial prefrontal cortical neurons synapsing onto striatal MSNs during action potential firing at frequencies that induce synaptic plasticity. mEPSC recordings from individual MSNs showed two distinct mEPSCs, higher amplitude, low-frequency and longer inter-event interval (group 1) and the lower amplitude, high-frequency and reduced inter-event interval (group 2), implying the sensitivity of whole-cell recordings to measure synaptic properties of MSNs.

Mutants exhibit grooming, anxiety and social behavioral impairment. Fluoxetine alleviates grooming, anxiety and social deficits in mutants similar to *Sapap3*-, *Slitrk5*- and *Shank3*-based OCD/ASD mouse models and human OCD patients.[7,25–32]

A direct correlation of immune dysfunction and neuropsychiatric disorders is observed in major depression, OCD, autism, schizophrenia and Alzheimer's disease.[33–44] Consequences of *Hoxb8* gene deficiency that results in corticostriatal synaptic aberration provides an independent way that the brain appear to utilize, to mediate and modulate repetitive behaviors. Interestingly, the loss of *Hoxb8* gene function that results in excessive grooming behavior was not restricted to repetitive behaviors since we detected fluoxetine-sensitive hyperanxiety and social behavioral deficit in *Hoxb8* mutants similar to trichotillomania-type OCD patients.[31,32,44–46]

Although the causative agents of the neuropsychiatric disorder in *Hoxb8*-mutant mice versus *Sapap3*, *Slitrk5* and *Shank3* mutant mice are very different, defective microglia versus defective synaptic components, the end results, both in terms of behavioral deficits, including high levels of anxiety and the affected neural circuits, the corticostriatal interface, are very similar. These results strongly support the hypothesis that in the absence of proper maintenance of circuit modulation by Hoxb8-microglia, very similar neural circuit damage ensues in *Hoxb8*, *Sapap3*, *Slitrk5* and *Shank3* mutant mice, resulting in very similar behavioral pathology.

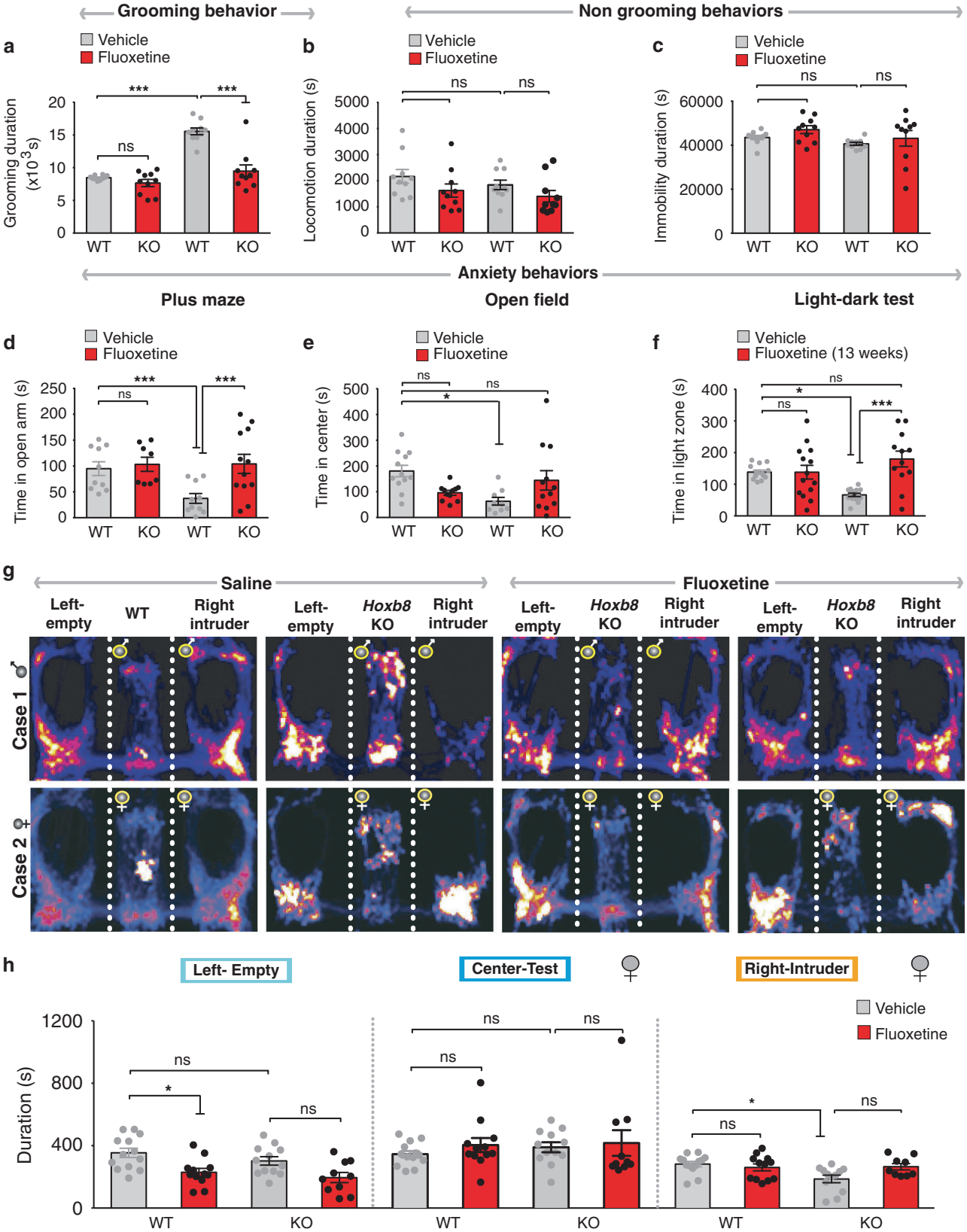

Hoxb8 gene thus appears to play an important role in maintaining brain homeostasis in regulating corticostriatal circuit function and behavioral output. *Hoxb8* gene dysfunction would alter synaptic morphology and physiological properties and thereby affect behaviors, the output of which would depend on the constellation of genetic and environmental insults pertinent to individual patient. Such models tie together immune dysfunctions, particularly pertaining to *Hoxb8* gene function through microglia,[25,47–52] the brain's immune system, with repetitive and anxiety behaviors and a spectrum of neuropsychiatric disorders.

Figure 4. Rescue of grooming, anxiety and social behaviors by chronic fluoxetine treatment. (**a**) Rescue of grooming behavior in age- and sex-matched *Hoxb8* mutants (6–12 months) treated with 5 mg kg^{-1} fluoxetine in post 5 week treated *Hoxb8* mutants ($P = 0.0001$, F(1, 36) = 18.95 for interaction; $P < 0.0001$, F(1, 36) = 32.43 for drug; $P < 0.0001$, F(1,36) = 54.23 for genotype). (**b** and **c**) 5-week treatment did not affect locomotion (**b**, $P = 0.8259$, F(1, 36) = 0.04911 for interaction; $P = 0.0434$, F(1, 36) = 4.385 for drug; $P = 0.2486$, F(1,36) = 1.375 for genotype) and immobility duration (**c**, $P = 0.8108$, F(1, 36) = 0.05817 for interaction; $P = 0.1552$, F(1,36) = 2.108 for drug; $P = 0.1074$, F(1,36) = 2.726 for genotype) significantly in mutants. (**d** and **e**) Five-week treated mutants show increased time in the open arm and the center of the open field. Complete rescue was observed in the plus maze test (**d**, $P = 0.0595$, F(1,36) = 3.788 for interaction; $P = 0.0170$, F(1,36) = 6.261 for drug; $P = 0.0675$, F(1,36) = 3.554 for genotype) but a partial rescue was noted in the open field test (**e**, $P = 0.0022$, F(1,36) = 10.71 for interaction; $P = 0.9404$, F(1,36) = 0.005653 for drug; $P = 0.1790$, F(1,36) = 1.871 for genotype). (**f**) Thirteen weeks treated *Hoxb8* mutants spend more time similar to WT mice in the light zone as compared to untreated mutants in 5 min light–dark test ($P = 0.0013$, F(1, 49) = 11.56 for interaction; $P = 0.0014$, F(1,49) = 11.50 for drug; $P = 0.3651$, F(1,49) = 0.8359 for genotype). (**g**) Representative heat maps of saline- and fluoxetine-treated male and female WT and *Hoxb8* mutants (Case 1–2) during three-chambered social interaction assay with an empty left chamber and an intruder in the right chamber (same sex as test mouse). Rescue of social interaction is more prominent in female *Hoxb8* mutants. (**h**) *Hoxb8* mutants show WT-like interaction time with the intruder mouse post two-week fluoxetine treatment in three-chambered social interaction test. The experimental female mouse was placed in the center chamber. The left chamber was left empty and the right chamber consisted of an intruder mouse of same sex as the experimental mouse ($P = 0.7438$, F(1, 43) = 0.1082 for interaction; $P = 0.0002$, F(1,43) = 16.45 for drug; $P = 0.1429$, F(1,49) = 2.227 for genotype for the time in left chamber; $P = 0.7295$, F(1, 43) = 0.1211 for interaction; $P = 0.3615$, F(1,43) = 0.8509 for drug; $P = 0.5411$, F(1,49) = 0.3796 for genotype for the time in the center chamber; $P = 0.1147$, F(1, 43) = 2.593 for interaction; $P = 0.5048$, F(1,43) = 0.4523 for drug; $P = 0.0126$, F(1,49) = 6.776 for genotype for the time in the right chamber). 6–12 months old age-matched WT and *Hoxb8* mutants were used for the experiments.

CONFLICT OF INTEREST

The authors declare no conflict of interest.

ACKNOWLEDGMENTS

We thank A Boulet and K Higgins for insightful discussions on the manuscript and editing, SK Chen for experimental discussion, H Eldering, BV Metris, for technical support, S Matsuoka for genotyping, and A Gosdis and V Krishnegowda for their participation in early experiments. This work was supported by Seed grant and research instrumentation funding from University of Utah to NN and MRC, HHMI, NIH/NEI, EY02576-36, EY015128-8 and EY014800-08 (P30) to BWJ and RM.

REFERENCES

1 Sachs BD. The development of grooming and its expression in adult animals. *Ann N Y Acad Sci* 1988; **525**: 1–17.
2 Graybiel AM, Saka E. A genetic basis for obsessive grooming. *Neuron* 2002; **33**: 1–2.
3 Greer JM, Capecchi MR. Hoxb8 is required for normal grooming behaviour in mice. *Neuron* 2002; **33**: 23–34.
4 Chen SK, Tvrdik P, Peden E, Cho S, Wu S, Spangrude G *et al.* Hematopoietic origin of pathological grooming in Hoxb8 mutants. *Cell* 2010; **141**: 775–785.
5 Graybiel AM, Rauch SL. Toward a neurobiology of obsessive-compulsive disorder. *Neuron* 2000; **28**: 343–347.
6 Graybiel AM. Habits, rituals, and the evaluative brain. *Annu Rev Neurosci* 2008; **31**: 359–387.
7 Fineberg NA, Chamberlain SR, Hollander E, Boulougouris V, Robbins TW. Translational approaches to obsessive-compulsive disorder: from animal models to clinical treatment. *Br J Pharmacol* 2011; **164**: 1044–1061.
8 Di Martino A, Kelly C, Grzadzinski R, Zuo XN, Mennes M, Mairena MA *et al.* Aberrant striatal functional connectivity in children with autism. *Biol Psychiatry* 2011; **69**: 847–856.
9 Welch JM, Lu J, Rodriguiz RM, Trotta NC, Peca J, Ding JD *et al.* Cortico-striatal synaptic defects and OCD-like behaviours in Sapap3-mutants. *Nature* 2007; **448**: 894–900.
10 Shmelkov SV, Hormigo A, Jing D, Proenca CC, Bath KG, Milde T *et al.* Slitrk5 deficiency impairs corticostriatal circuitry and leads to obsessive-compulsive-like behaviours in mice. *Nat Med* 2010; **16**: 598–602.
11 Peca J, Feliciano C, Ting JT, Wang W, Wells MF, Venkatraman TN *et al.* Shank3 mutants display autistic-like behaviours and striatal dysfunction. *Nature* 2011; **472**: 437–442.
12 Menzies L, Chamberlain SR, Laird AR, Thelen SM, Sahakian BJ, Bullmore ET. Integrating evidence from neuroimaging and neuropsychological studies of obsessive-compulsive disorder: the orbitofronto-striatal model revisited. *Neurosci Behav Rev* 2008; **32**: 525–549.
13 Beucke JC, Sepulcre J, Talukdar T, Linnman C, Zschenderlein K, Endrass T *et al.* Abnormally high degree connectivity of the orbitofrontal cortex in obsessive-compulsive disorder. *JAMA Psychiatry* 2013; **70**: 619–629.
14 Ahmari SE, Spellman T, Douglass NL, Kheirbek MA, Simpson HB, Deisseroth K *et al.* Repeated cortico-striatal stimulation generates persistent OCD-like behaviour. *Science* 2013; **340**: 1234–1239.
15 Schmeisser MJ, Ey E, Wegener S, Bockmann J, Stempel AV, Kuebler A *et al.* Autistic-like behaviours and hyperactivity in mice lacking ProSAP1/Shank2. *Nature* 2012; **486**: 256–260.
16 Shepherd GM. Corticostriatal connectivity and its role in disease. *Nat Rev Neurosci* 2013; **14**: 278–291.
17 Burguiere E, Monteiro P, Feng G, Graybiel AM. Optogenetic stimulation of lateral orbitofronto-striatal pathway suppresses compulsive behaviours. *Science* 2013; **340**: 1243–1246.
18 Geller DA, Hoog SL, Heiligenstein JH, Ricardi RK, Tamura R, Kluszynski S *et al.* Fluoxetine treatment for obsessive-compulsive disorder in children and adolescents: a placebo-controlled clinical trial. *J Am Acad Child Adolesc Psychiatry* 2001; **40**: 773–779.
19 Marc RE, Liu W. Fundamental GABAergic amacrine cell circuitries in the retina: nested feedback, concatenated inhibition, and axosomatic synapses. *J Comp Neurol* 2000; **425**: 560–582.
20 Chen YH, Harvey BK, Hoffman AF, Wang Y, Chiang YH, Lupica CR. MPTP-induced deficits in striatal synaptic plasticity are prevented by glial cell line-derived neurotrophic factor expressed via an adeno-associated viral vector. *FASEB J* 2008; **22**: 261–275.
21 Cordingley GE, Weight FF. Non-cholinergic synaptic excitation in neostriatum: pharmacological evidence for mediation by a glutamate-like transmitter. *Br J Pharmacol* 1986; **88**: 847–856.
22 Malenka RC, Kocsis JD. Presynaptic actions of carbachol and adenosine on corticostriatal synaptic transmission studied in vitro. *J Neurosci* 1988; **8**: 3750–3756.
23 Quinn LP, Stean TO, Chapman H, Brown M, Vidgeon-Hart M, Upton N *et al.* Further validation of LABORAS using various dopaminergic manipulations in mice including MPTP-induced nigro-striatal degeneration. *J Neurosci Methods* 2006; **156**: 218–227.
24 Diefenbach GJ, Tolin DF, Hannan S, Crocetto J, Worhunsky P. Trichotillomania: impact on psychosocial functioning and quality of life. *Behav Res Ther* 2005; **43**: 869–884.
25 Frick LR, Williams K, Pittenger C. Microglial dysregulation in psychiatric disease. *Clin Dev Immunol* 2013; **2013**: 608654.
26 Krebs G, Heyman I. Obsessive-compulsive disorder in children and adolescents. *Arch Dis Childhood* 2014; **100**: 495–499.
27 Gkogkas CG, Khoutorsky A, Ran I, Rampakakis E, Nevarko T, Weatherill DB *et al.* Autism-related deficits via dysregulated eIF4E-dependent translational control. *Nature* 2013; **493**: 371–377.
28 Han S, Tai C, Westenbroek RE, Yu FH, Cheah CS, Potter GB *et al.* Autistic-like behaviour in Scn1a+/- mice and rescue by enhanced GABA-mediated neurotransmission. *Nature* 2012; **489**: 385–390.
29 Moore ML, Eichner SF, Jones JR. Treating functional impairment of autism with selective serotonin-reuptake inhibitors. *Ann Pharmacol* 2004; **38**: 1515–1519.
30 Hollander E, Phillips A, Chaplin W, Zagursky K, Novotny S, Wasserman S *et al.* A placebo controlled crossover trial of liquid fluoxetine on repetitive behaviours in childhood and adolescent autism. *Neuropsychopharmacology* 2005; **30**: 582–589.
31 Koran LM, Ringold A, Hewlett W. Fluoxetine for trichotillomania: an open clinical trial. *Psychopharmacol Bull* 1992; **28**: 145–149.
32 Rossi A, Barraco A, Donda P. Fluoxetine: a review on evidence based medicine. *Ann Gen Hosp Psychiatry* 2004; **3**: 2.

33 Ashwood P, Wills S, Van de Water J. The immune response in autism: a new frontier for autism research. *J Leukoc Biol* 2005; **80**: 1–15.
34 Da Rocha FF, Correa H, Teixeira AL. Obsessive-compulsive disorder and immunology: a review. *Prog Neuropsychopharmacol Biol Psychiatry* 2008; **32**: 1139–1146.
35 Kronfol Z, Remick DG. Cytokines and the brain: implications for clinical psychiatry. *Am J Psychiatry* 2000; **157**: 683–694.
36 Lang UE, Puls I, Muller DJ, Strutz-Seebohm N, Gallinat J. Molecular mechanisms of schizophrenia. *Cell Physiol Biochem* 2007; **20**: 687–702.
37 Leonard BE, Myint A. The psychoneuroimmunology of depression. *Hum Psychopharmacol* 2009; **24**: 165–175.
38 Strous RD, Shoenfeld Y. Schizophrenia, autoimmunity and immune system dysregulation: a comprehensive model updated and revisited. *J Autoimmun* 2006; **27**: 71–80.
39 Hounie AG, Cappi C, Cordeiro Q, Sampaio AS, Moraes I, Rosario MC *et al.* TNF-alpha polymorphisms are associated with obsessive-compulsive disorder. *Neurosci Lett* 2008; **442**: 86–90.
40 Purcell SM, Wray NR, Stone JL, Visscher PM, O'Donovan MC, Sullivan PF *et al.* Common polygenic variation contributes to risk of schizophrenia and bipolar disorder. *Nature* 2009; **460**: 748–752.
41 Shi J, Levinson DF, Duan J, Sanders AR, Zheng Y, Pe'er I *et al.* Common variants on chromosome 6p22.1 are associated with schizophrenia. *Nature* 2009; **460**: 753–757.
42 Stefansson H, Ophoff RA, Steinberg S, Andreassen OA, Cichon S, Rujescu D *et al.* Common variants conferring risk of schizophrenia. *Nature* 2009; **460**: 744–747.
43 Luthi A, Lüscher C. Pathological circuit function underlying addiction and anxiety disorders. *Nat Neurosci* 2014; **12**: 1635–1643.
44 Markarian Y, Larson MJ, Aldea MA, Good D, Berkeljon A, Murphy TK *et al.* Multiple pathways to functional impairment in obsessive-compulsive disorder. *Clin Psychol Rev* 2010; **30**: 78–88.
45 Sakai Y, Narumoto J, Nishida S, Nakamae T, Yamada K, Nishimura T *et al.* Corticostriatal functional connectivity in non-medicated patients with obsessive-compulsive disorder. *Eur Psychiatry* 2011; **26**: 463–469.
46 Harrison BJ, Soriano-Mas C, Pujol J, Ortiz H, López-Solà M, Hernández-Ribas R *et al.* Altered corticostriatal functional connectivity in obsessive-compulsive disorder. *Arch Gen Psychiatry* 2009; **66**: 1189–1200.
47 Ransohoff RM, Liu L, Cardona AE. Chemokines and chemokine receptors: multipurpose players in neuroinflammation. *Int Rev Neurobiol* 2007; **82**: 187–204.
48 Stevens B, Allen NJ, Vazquez LE, Howell GR, Christopherson KS, Nouri N *et al.* The classical complement cascade mediates CNS synapse elimination. *Cell* 2007; **131**: 1164–1178.
49 Ransohoff RM, Cardona AE. The myeloid cells of the central nervous system parenchyma. *Nature* 2010; **468**: 253–262.
50 Paolicelli RC, Bolasco G, Pagani F, Maggi L, Scianni M, Panzanelli P *et al.* Synaptic pruning by microglia is necessary for normal brain development. *Science* 2011; **333**: 1456–1458.
51 Prinz M, Priller J, Sisodia SS, Ransohoff RM. Heterogeneity of CNS myeloid cells and their roles in neurodegeneration. *Nat Neurosci* 2011; **14**: 1227–1235.
52 Schafer DP, Lehrman EK, Kautzman AG, Koyama R, Mardinly AR, Yamasaki R *et al.* Microglia sculpt postnatal neural circuits in an activity and complement-dependent manner. *Neuron* 2012; **74**: 691–705.
53 Anderson JR, Jones BW, Yang JH, Shaw MV, Watt CB, Koshevoy P *et al.* A computational framework for ultrastructural mapping of neural circuitry. *PLoS Biol* 2009; **7**: e1000074.

Supplementary Information accompanies the paper on the Molecular Psychiatry website (http://www.nature.com/mp)